Proceedings of the 10th International Conference on Fluid Flow, Heat and Mass Transfer (FFHMT'23)
Canada – June 07-09, 2023
Paper No. 110
DOI: 10.11159/ffhmt23.110

Heat Transfer Analysis of a Crossflow Minichannel Heat Exchanger Based on Air and Liquid Flow Implementing PCM as Latent Heat Thermal Energy Storage

Mahdi Momeni[1], Saman Jalilian[1], Amir Fartaj[1]
Department of Mechanical, Automotive, and Materials Engineering, University of Windsor,
401 Sunset Ave, Windsor, Ontario, Canada
mahdimo@uwindsor.ca, jalilas@uwindsor.ca, fartaj@uwindsor.ca

Abstract **-** Due to mismatches between energy supply and demand in thermal systems, this paper introduces an innovative phase change material (PCM) heat exchanger based on two working fluids to provide thermal energy storage for the airside. The PCM is integrated into a compact single-slabbed crossflow heat exchanger based on air and liquid flow. A numerical heat transfer and fluid flow analysis is conducted based on a three-dimensional computational fluid dynamics (CFD) simulation of the model. The dynamic thermal performance of the system is demonstrated for both the PCM charging and discharging processes. Due to the results attained, the PCM can store excess heat in the charging process, which is then released to the airside during periods of demand when the system hot working fluid is unavailable. In the discharge process, the stored thermal energy provides the airside with a heating load of 118 kJ and up to 150 seconds of heating time. The findings attained in this study will shed light on the development of PCM heat exchangers.

Keywords**:** PCM heat exchanger; Thermal energy storage; Thermal management; Air and liquid flow; Phase change material

Nomenclature

$\vec{g}$	gravitational acceleration (m/s^2)
H	total enthalpy (J)
k	thermal conductivity (W/m^2.K)
P	pressure (Pa)
$\vec{S}$	source term of momentum (m/s)
T	temperature (^{o}C)

Abbreviations

2D	two-dimensional
3D	three-dimensional
CAD	computer-aided design
CFD	computational fluid dynamics
LHTES	latent heat thermal energy storage
PCM	phase change material
TES	thermal energy storage

Greek symbols

β	thermal expansion coefficient (1/K)
ρ	density (kg/m^3)
μ	dynamic viscosity (Pa/s)
∇	gradient operator

Subscripts

ref	reference state

1. Introduction

Increasing global economic growth and new sectors have led to a noticeable rise in energy consumption [1]. Among the most important forms of energy, heat is used daily in domestic, commercial, transportation, and industrial settings [2]. Heat exchangers are considered to be the most crucial component of thermal systems, and their performance influences the entire system's performance [3]. Research has focused on improving heat exchanger thermal characteristics. As a viable solution, incorporating latent heat thermal energy storage (LHTES) of phase change materials (PCMs) in thermal systems has attracted attention in previous research [4]. When PCM is used to store energy within a heat exchanger, LHTES can be stored or released to reduce peak energy demands or provide additional cooling and heating for thermal processes [5]. In order to ensure optimal heat transfer and energy efficiency from the heat exchanger, a transient analysis must be performed on the heat exchanger study [6]. Different types of heat exchangers have been developed over time, but crossflow heat exchangers have been used extensively in various tubular heat exchanger applications, and various experimental and numerical research has been conducted on these exchangers [7]. Thermal characteristics, compactness, and energy efficiency could be improved with an efficient heat exchanger design, such as using minichannels in a compact heat exchanger [8].

In recent years, there has been an increase in interest in the dynamic analysis of heat exchangers for applications that primarily involve heating or cooling to study the control of fluid outlet temperatures. In an experimental study, Fotowat et

al. [9] compared the performance of a conventional and meso heat exchanger when the inlet operation conditions were changed in a stepwise manner. The meso heat exchanger achieved a steady state earlier and exhibited significantly higher thermal efficiency than a conventional heat exchanger. A numerical study presented by Ismail et al. [10] focused on forced convection heat transfer simulations in sequential and simultaneous air-to-liquid crossflow heat exchangers. Compared to a sequential heat exchanger module, the second heat exchanger module showed significant improvements in heat transfer rates at a given Reynolds number. In another numerical study provided by the same author [11], the effects of circular channel diameter on the convective heat transfer and pressure drop behaviour within thin slabs minichannel heat exchangers was analysed. According to their findings, pressure drop changes decrease with increasing channel diameter and decreasing Reynolds number. However, for larger diameters and lower Reynolds numbers, there is no significant change in pressure drop.

As discussed in the above literature review, the dynamic analysis provides insight into the heat exchanger's thermal behaviour. As a gap in the literature regarding transient analysis of heat exchangers, using LHTES could enhance conventional heat exchangers and provide sustainable thermal management for these systems. Implementing PCM can provide a sustainable energy system and improve overall efficiency due to its ability to manage heat and provide adequate thermal energy. In this regard, this study aims to integrate PCM as thermal energy storage in a compact single slabbed finned air-and liquid heat exchanger to provide a sustainable energy storage method. The PCM stores excess heat of the liquid in the charging process. The PCM reliably extends the operating period when the main fluid is temporarily turned off at shutdown time to minimize the need for an external power source or batteries. A complete heat transfer analysis is provided, and the dynamic behaviour of the operational fluids and the PCM is studied.

2. Numerical Methodology

To conduct the numerical simulations of the study, three-dimensional (3D) computational fluid dynamics (CFD) is performed based on the finite element method using COMSOL Multiphysics® 6.0 commercial software. The detail of the numerical modelling is presented in the sections below.

2.1. Geometry modelling

The conventional heat exchanger model is based on a single slab finned air-liquid heat exchanger equipped with minichannel liquid flow operation and PCM. The computer-aided design (CAD) model of the system is represented in Fig. 1. The heat exchanger is aluminium material for the body and has two rows of fins above and under the main slab. The PCM is placed through the top row of the heat exchanger between the fins. Hot water inserts the heat exchanger liquid side and distributes through 68 minichhanals inside the slab. The heat exchanger is placed inside the air channel domain seen in Fig. 1 (b), which allows the air to pass through the heat exchanger slabs through the bottom fins row and exchange heat with the hot water and the PCM domain. Effective extensive surfaces (fins) are distributed within the PCM domain and between the heat exchanger slabs to enhance the PCM's thermal performance and ensure an efficient heat transfer to the fluids. The design specifications of the PCM heat exchanger are presented in Table 1.

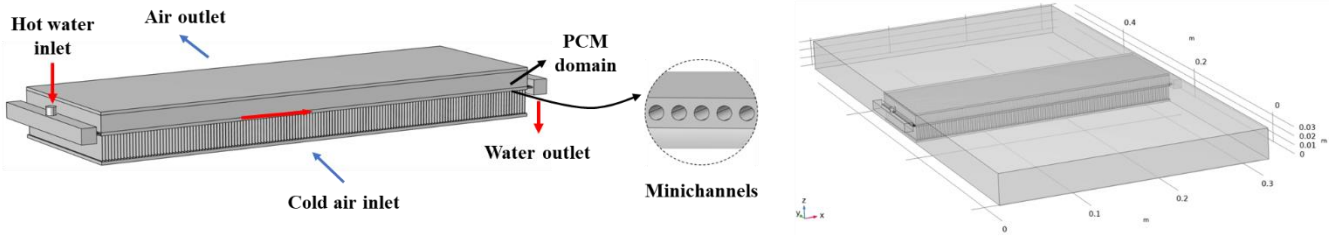

a) Minichannal heat exchanger

b) Heat exchanger inside air domain

Fig. 1: CAD design of the PCM heat exchanger.

Table 1: Design specifications of the single slabbed PCM heat exchanger based on [12].

Specifications	Value
Number of channels in the slab	68
Slab length (mm)	305
Slab width (mm)	100
Slab height (mm)	2
Channel diameter (mm)	1
Fin density (fins per inch)	12

Specifications	Value
Fin height – top row (mm)	10.65
Fin height – bottom row (mm)	15.79
Fin thickness (mm)	1.85
Number of fins per row	144
Air channel dimensions (mm)	$34 \times 305 \times 600$
Heat exchanger material	Aluminium

2.2. Operational Setup and Assumptions

The presented heat exchanger based on two operational fluids and PCM storage is designed to provide heating for the airside based on hybrid heat sources of water and the PCM. The hot fluid material is selected water, with an inlet temperature of 70 ^{o}C and a mass flow rate of 30 g/s. In the airside, constant inlet temperature and air stream velocity are selected at 13 ^{o}C and 2 m/s, respectively. The initial temperature of the model simulation was selected at 20 ^{o}C. The entire system was divided into four main domains and materials: aluminium for the heat exchanger domain, water for the channels of the heat exchanger, air for the air channel, and PCM for its designated domain.

The system simulation is presented for the PCM's charging and discharging process. In the charging process, the hot water passes through the heat exchanger slab, melting the solid PCM while heating the air. The water circulation is shut down during the discharging process, enabling the air to extract the latent heat stored in the melted PCM, thereby delaying the air temperature drop and ensuring a warm air outlet. LTHES provides reliable and sustainable heat storage for use during liquid shutdown periods of the heat exchanger.

The following assumptions have been made for the system flows and boundary conditions of the system:

- The fluids are single-phase and incompressible
- The thermodynamic properties of aluminum are constant, but air and water are temperature dependent. For the PCM, thermodynamic properties are constant within a constant phase
- There is a laminar flow regime in the water and a turbulent flow regime in the air
- A uniform and homogeneous mass is assumed for the PCM
- Thermal insulation is considered for the walls of the air domain
- The system does not transfer heat by diffusion or radiation

2.3. PCM Selection

In thermal management and TES applications, paraffin based PCMs are extensively used since they have a broad melting temperature range. As a result of its appropriate melting temperature, Docosane is used in this study to accomplish air heating within the heat exchanger's air and liquid sides. Table 2 summarizes the thermophysical properties of the selected PCM.

Table 2: PCM thermophysical properties [13].

Material properties	Value
Commercial name	Docosane
Melting temperature (°C)	43.80
Latent heat of fusion (kJ/kg)	234
Average density (kg/m3)	820

Material properties	Value
Specific heat (solid) (J/kg.°C)	1700
Specific heat (liquid) (J/kg.°C)	2200
Thermal conductivity (solid) (W/m.°C)	0.37
Thermal conductivity (liquid) (W/m.°C)	0.24

2.4. Mesh Grid Generation

The heat exchanger domains have been divided into several sub-domains: air, liquid channels, and solids (fins and slabs). For the sub-domains of the designed model, free tetrahedral meshes were used to generate mesh grids. In order to discretize the small geometry regions of the heat exchanger, more refined elements were used. Three boundary layers were considered

for the inlet and outlet of the water and air boundaries. To examine the grid dependence of the results, a mesh convergence test is conducted to attain high-quality CFD results. The total grid element number of 1.40×10^6 is used in the model with an average element quality of 0.31. Fig. 2 shows the final meshed geometry for the complete PCM heat exchanger, including the air, PCM, slabs, fins, and water channel domains.

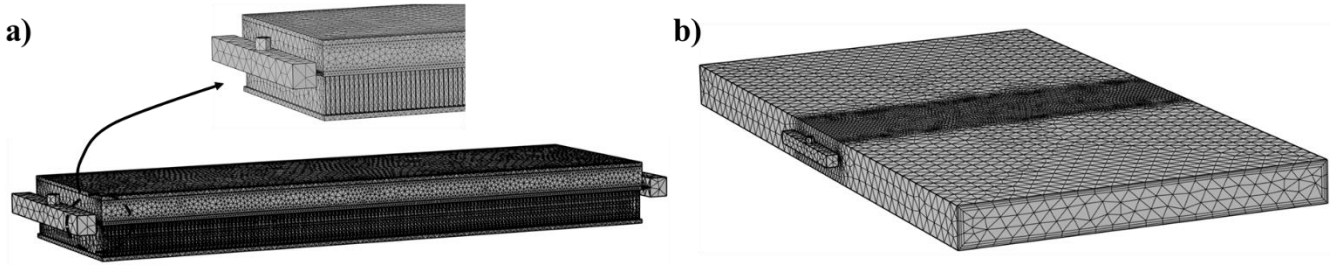

Fig. 2: Mesh grid generated for the PCM heat exchanger (a) minichannel heat exchanger (b) air domain.

2.5. Governing Equations

Based on the assumptions and model developed in COMSOL Multiphysics, the following main equations are solved in the simulations:

Mass conservation:

$$\frac{\partial \rho}{\partial t} + \nabla.(\rho \vec{V}) = 0 \tag{1}$$

Momentum conservation:

$$\rho \frac{\partial \vec{V}}{\partial t} + \rho(\nabla.\vec{V})\vec{V} = -\nabla P + \mu(\nabla^2 \vec{V}) + \rho_{ref}\beta(T - T_{ref})\vec{g} + \vec{S} \tag{2}$$

Energy conservation:

$$\frac{\partial(\rho H)}{\partial t} + \nabla(\rho H \vec{V}) = \nabla(k\nabla T) \tag{3}$$

Where in Eq. (2), $\vec{S}$ is the Darcy source term which is based on the variation in porosity of the mushy zone. Besides these equations, the software calculates the total latent heat and sensible heat of the PCM. Also, the liquid fraction of the mushy zone is determined to calculate the latent heat share. The thermophysical properties of the PCM at any state is calculated based on the properties provided to the software and the liquid fraction of the PCM. After defining the thermophysical properties of the PCM during phase change, it is possible to solve the energy equation using the apparent heat capacity method.

2.6. Computational Setup and Boundary Conditions

For modelling the physics of the study, laminar flow is used for the water domain, and turbulent flow based on $k-\varepsilon$ model is used for the air domain. Heat transfer in solid and liquids physics is performed on the model to attain complete thermal behaviour of the operating fluids and the PCM. The heat transfer and flow physics are coupled in a Multiphysics simulation. The convective and diffusive terms were approximated using Symmetric Interior Penalty Galerkin (SIPG), and the time derivative was approximated using Backward Differentiation (BDF).

The following boundary conditions were applied for the model simulation:

- Heat transfer liquid and air inlet: average mass flow rate inlet, upstream constant temperature flow inlet
- Heat transfer liquid and air outlet: constant pressure condition

- Air tunnel outer walls: thermal insulation
- Heat exchanger body and heat transfer liquid interior walls: no-slip wall, thermal coupling

3. Results and Discussion

This section presents the numerical results of air heating integrated with TES using latent heat in a PCM heat exchanger. An analysis of the effects of the PCM inside the model is conducted using the operational conditions. The results provide an insight into the response of the charging and discharging processes and the effect of the PCM LTES on extending the heating period to the airside. Several parameters, such as the fluids outlet temperature, the PCM average temperature, and the fluid heat transfer rate, are discussed in this section.

3.1. Dynamic Simulation Results

The CFD model simulated the charging and discharging processes for the operational conditions mentioned. The simulation covered 200 seconds for both processes, with the charging process from $t = 0 - 200$ s and discharging process from $t = 200 - 400$ s. This time interval was found adequate to achieve a steady-state situation for both processes.

Fig. 3 shows the transient plots of fluids outlet temperature, PCM average temperature, and solid fraction during the processes. The temperatures started from 20°C, and during the charging process, the water heated the air while melting the PCM. At the end of the charging process, the outlet temperature of the water reached approximately 54°C. The system temperatures reached a steady state at around 120 seconds, and the PCM was almost completely melted, with a solid fraction of 0.02.

The discharging process began by shutting down the water inlet at $t = 200$ s, which allowed the thermal energy stored in the PCM to be extracted. The air outlet and PCM average temperatures initially dropped significantly with a sharp slope. After reaching the solidification temperature of the PCM, latent heat activated, allowing high heat transfer rates to the air. This delayed the cooling of the airside, and at around around $t = 300$ s, the PCM was fully melted. The PCM and air outlet temperature reached a steady state of 13°C at the end of the discharge process, and the LHTES provided additional air heating for around 150 seconds.

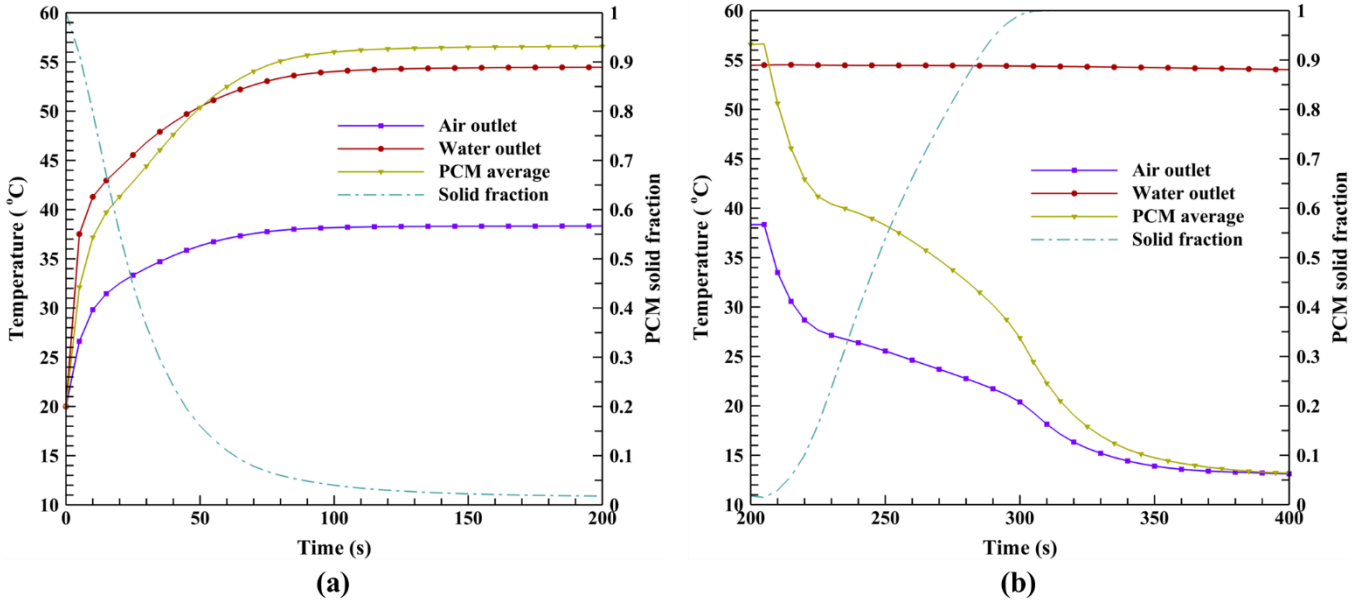

Fig. 3: Dynamic plots for the operation fluids and PCM for (a) charging process (b) discharging process.

An illustration of the transient behaviour of the airside heat transfer rate during the charging and discharging process along with the heat transfer rate of water during the charging process is provided in Fig. 4. It is observed that the water side heat transfer dops in the charging process, starting from 6.3 kW and reaching to 1.9 kW at the final stage. This is because the water is cooled down during the charging process, heating up the air and melting the PCM to store latent heat. The integration through the heat rate plot of charging heat is provided, which is the total amount of heat transferred from the hot water to the cold air and PCM during the charging process. This amount is calculated and attained at 467.7 kJ. Observing the airside heat rate plot for the charging process, it is evident that the airside heat transfer starts at a low amount and increases to around 1.9 kW at the end of the process. This is because the air is heating in the charging process, and the air outlet temperature is increasing. The total heat that the airside attained from the hot fluid in the charging process is achieved at 364.9 kJ. By subtracting this amount from the total charging heat, 102.7 kJ of energy is attained. Considering no heat losses, this amount is the heat stored in the PCM during the charging process. This energy is later provided to heat the airside in the discharge process. Looking at the airside heat transfer during the discharge process, it is seen that the trend drops while the cold air fully resolidifies the PCM. The amount of energy the charged PCM and the heat exchanger body provide to the air in the discharge process is calculated as 117.9 kJ. This quantity represents the heat that can be delivered to the airside during the discharge process when the hot fluid is shut down, indicating the impact of the PCM's LHTES

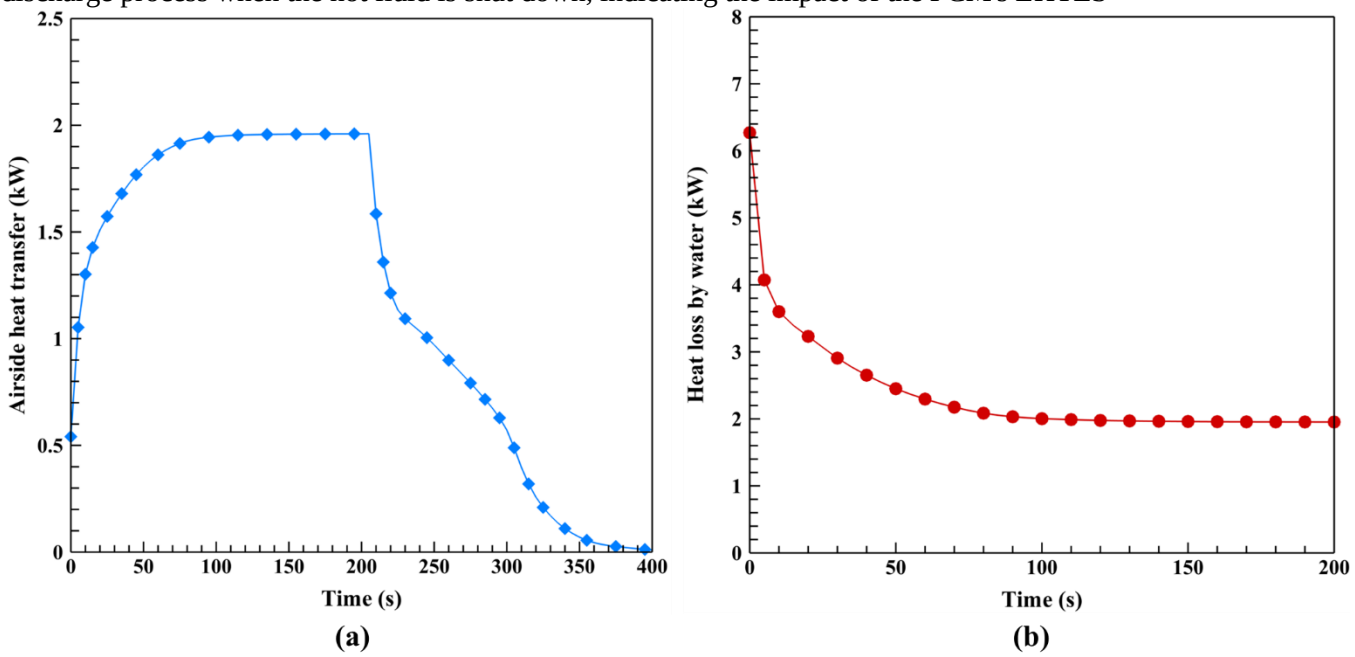

Fig. 4: Fluids heat transfer rates (a) airside heat transfer for charging and discharging process (b) waterside heat transfer for charging process.

3.2. PCM Phase Transition Procedure

To represent the melting and solidification procedure of the PCM during the charging and discharging processes, the 2D phase fraction CFD results of the PCM during different simulation times are illustrated in Fig. 5. Graphic solid fraction contours are provided for a cut plain in the middle section inside the PCM domain. It is observed from the charging process contours that the PCM melting phenomena is initially occurring faster around the inlet of the water, which is the left and under the PCM domain. The number of 144 thin fins distributed inside the PCM domain highly affects the melting and solidification procedure. Heat is distributed from the hot water by convective heat transfer through fins inside the PCM domain. The PCM plane is gradually melting in the charging process, reaching an almost fully melted position after 60 seconds of operation. The PCM domain's lower side is melting slower due to the cold air being in contact and passing underneath the PCM domain.

In the discharging process, it can be observed that while air is flowing underneath the PCM block, solidification occurs gradually from the lower to the higher regions of the domain. During convective heat transfer, cold energy from air facing beneath the domain is distributed inside the PCM block through the fins. The process of PCM solidification with airflow takes a higher time in contrast with the PCM melting with the liquid flow during the charging process. After 80 seconds of discharge time, the PCM plane has reached an almost entirely solidified situation.

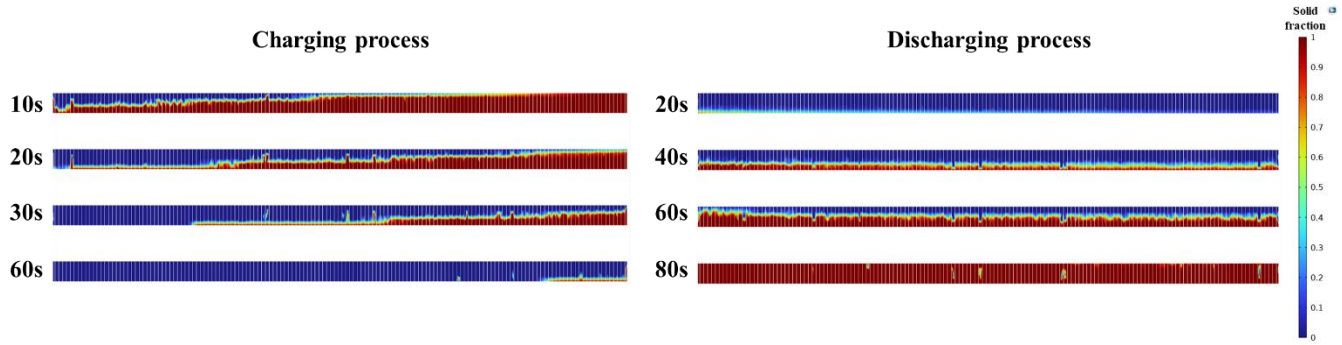

Fig. 5: Phase fraction contours of the PCM melting and solidification process.

4. Conclusion

In this paper, a single slabbed crossflow heat exchanger based on air and liquid flow is equipped with PCM with the purpose of storage of thermal energy to provide additional airside heating during liquid shutdown periods. The following conclusions are drawn from the results attained:

- In the charging process, the hot water flow fully melts the PCM providing energy storage of 103 kJ for the heat exchanger. This thermal energy stored is released to the airside during the discharge process to maintain air heating.
- Regarding the discharge process, the PCM heat exchanger provides 118 kJ of additional heat to the airside resulting in around 150 seconds of extra air heating.
- The thin fins distributed inside the PCM domain highly improve the thermal performance and heat transfer process during the melting and solidification.
- The PCM melting process with the hot water flow occurs faster than the PCM solidification time using the cold airflow. The PCM melting and solidification times are attained at around 80 and 100 seconds, respectively.

Acknowledgements

This work was supported by the Natural Sciences and Engineering Research Council of Canada (NSERC) offered at the University of Windsor.

References

[1] M. Momeni, M. Soltani, M. Hosseinpour, J. Nathwani. A comprehensive analysis of a power-to-gas energy storage unit utilizing captured carbon dioxide as a raw material in a large-scale power plant. Energy Conversion and Management. 227 (2021) 113613.

[2] M. Momeni, S. Jani, A. Sohani, S. Jani, E. Rahpeyma. A high-resolution daily experimental performance evaluation of a large-scale industrial vapor-compression refrigeration system based on real-time IoT data monitoring technology. Sustainable Energy Technologies and Assessments. 47 (2021) 101427.

[3] H. Li, N. Wang, B. Zhao, H. Feng, K. Han, S. He, M. Gao. Simulation study on the effect of fins on the heat transfer performance of horizontal dual-inner-tube latent thermal energy storage heat exchangers. Journal of Energy Storage. 49 (2022) 104125.

[4] L. Kalapala, J.K. Devanuri. Influence of operational and design parameters on the performance of a PCM based heat exchanger for thermal energy storage – A review. Journal of Energy Storage. 20 (2018) 497-519.
[5] S. Rana, M. Zunaid, R. Kumar. CFD analysis for heat transfer comparison in circular, rectangular and elliptical tube heat exchangers filled with PCM. Materials Today: Proceedings. 56 (2022) 637-44.
[6] S. Askar, S. Fotowat, A. Fartaj. Transient experimental investigation of airside heat transfer in a crossflow heat exchanger. Applied Thermal Engineering. 199 (2021) 117516.
[7] C.K. Mangrulkar, A.S. Dhoble, S. Chamoli, A. Gupta, V.B. Gawande. Recent advancement in heat transfer and fluid flow characteristics in cross flow heat exchangers. Renewable and Sustainable Energy Reviews. 113 (2019) 109220.
[8] F.A. Siddiqui, E.S. Dasgupta, A. Fartaj. Experimental investigation of air side heat transfer and fluid flow performances of multi-port serpentine cross-flow mesochannel heat exchanger. International Journal of Heat and Fluid Flow. 33 (2012) 207-19.
[9] S. Fotowat, S. Askar, A. Fartaj. Experimental transient response of a minichannel heat exchanger with step flow variation. Experimental Thermal and Fluid Science. 89 (2017) 128-39.
[10] M.S. Ismail, M. G. Khan, A. Fartaj. Investigation of Sequential and Simultaneous Crossflow Heat Exchangers for Automotive Application. 2020.
[11] M.S. Ismail, S. Fotowat, A. Fartaj. Effect of Channel Size on Heat Transfer and Pressure Drop in Thin Slabs Minichannel Heat Exchanger. 2014.
[12] S. Fotowat, S. Askar, A. Fartaj. Transient response of a meso heat exchanger with temperature step variation. International Journal of Heat and Mass Transfer. 122 (2018) 1172-81.
[13] S. Kahwaji, M.B. Johnson, A.C. Kheirabadi, D. Groulx, M.A. White. A comprehensive study of properties of paraffin phase change materials for solar thermal energy storage and thermal management applications. Energy. 162 (2018) 1169-82.